Published in final edited form as:
Dev Cell. 2008 April ; 14(4): 570–581. doi:10.1016/j.devcel.2008.03.003.

Collective Epithelial Migration and Cell Rearrangements Drive Mammary Branching Morphogenesis

Andrew J. Ewald[1,*], **Audrey Brenot**[1], **Myhanh Duong**[1], **Bianca S. Chan**[1], and **Zena Werb**[1,*]
[1]Department of Anatomy and Program in Cell Biology, University of California, San Francisco, San Francisco, CA 94143, USA

Summary

Epithelial organs are built through the movement of groups of interconnected cells. We observed cells in elongating mammary ducts reorganize into a multilayered epithelium, migrate collectively, and rearrange dynamically, all without forming leading cellular extensions. Duct initiation required proliferation, Rac, and myosin light-chain kinase, whereas repolarization to a bilayer depended on Rho kinase. We observed that branching morphogenesis results from the active motility of both luminal and myoepithelial cells. Luminal epithelial cells advanced collectively, whereas myoepithelial cells appeared to restrain elongating ducts. Significantly, we observed that normal epithelium and neoplastic hyperplasias are organized similarly during morphogenesis, suggesting common mechanisms of epithelial growth.

Introduction

A fundamental question in biology is, “how do cells collaborate to build and change the structure of epithelial tissues, while maintaining characteristically epithelial features such as cell-cell contact and barrier function” (Pilot and Lecuit, 2005)?

We chose to study branching morphogenesis in the mammary gland as a model to understand how the cells of a postnatal epithelial tissue collectively remodel the architecture of a tubular network. The mammary gland is particularly suited to such studies, as it develops in an ongoing, hormonally driven process throughout reproductive life (Sternlicht, 2006; Woodward et al., 2005). The majority of branching morphogenesis occurs during puberty (Figure 1A), but the mammary epithelium also remodels during each cycle of pregnancy, lactation, and involution (Hennighausen and Robinson, 2005).

Quiescent mammary ducts are bilayered (Figure 1B; Figure S1; see the Supplemental Data available with this article online) and consist of a luminal and myoepithelial layer in both mice and humans. Hyperplasias and carcinomas have a very different architecture, with many cell layers (Figure 1C), increased proliferation, partial loss of cell polarity, and reduced intercellular adhesion (Bilder, 2004). However, during puberty, terminal end buds (TEBs) form transiently at the end of each primary duct. TEBs are characteristically different from quiescent ducts: they have multiple luminal cell layers, are enriched in mammary stem cells, and have high levels of proliferation (Figures 1D and 1E; Figure S1) (Hinck and Silberstein, 2005; Williams and Daniel, 1983). The multilayered TEB gives rise to bilayered ducts, with myoepithelial

*Correspondence: andrew.ewald@ucsf.edu (A.J.E.), zena.werb@ucsf.edu (Z.W.).

Supplemental Data
Supplemental Data include three figures and seventeen movies and can be found online at http://www.developmentalcell.com/cgi/content/full/14/4/570/DC1/.

(ME) cells surrounding luminal epithelial (LE) cells (Figures S1A and S1A′). Despite advances in dissecting the genetic regulation of mammary development (Howlin et al., 2006), the cellular basis of ductal elongation and bifurcation remains obscure.

We sought to observe mammary epithelial cells during the initiation, elongation, and bifurcation of new ducts and to identify molecular pathways involved in regulating each of these processes. We used primary, organotypic three-dimensional (3D) culture and long-term confocal time-lapse analysis to show that mammary ducts elongate through a different type of collective epithelial migration, with no leading cell extensions or leading actin-rich protrusions. We then used pharmacologic perturbations to identify molecular regulators of ductal morphogenesis. Finally, we showed that, during morphogenesis, mammary epithelium is similarly organized in organotypic cultures, during ductal invasion in vivo, and in mouse mammary hyperplasias.

Results

Modeling Mammary Branching Morphogenesis in Organotypic Culture

Mammary ductal elongation in vivo occurs over the course of weeks, making it difficult to monitor directly. Accordingly, we imaged individual cells over time in an organotypic culture model of mammary branching morphogenesis (Fata et al., 2007; Simian et al., 2001; Sternlicht et al., 2005; Wiseman et al., 2003). We cultured fragments of freshly isolated mammary epithelium (organoids) in 3D Matrigel gels and collected over 200 bright-field movies and over 400 3D confocal movies to determine the basic sequence of events involved in branching morphogenesis. In minimal medium, the epithelial pieces all formed “simple cysts” with a bilayered organization and a clear lumen (Figure 1H). Addition of FGF2 to the medium induced initiation and elongation of new ducts (Movie S1). We considered an organoid branched if it had three ducts, as previously established (Fata et al., 2007). There was no correlation between the initial structure of the organoid and the sites of ductal initiation in culture.

Keratin-14-GFP-Actin Mice Enable Dynamic Visualization of Myoepithelial Cell Behavior

In vivo, the mammary epithelium consists of keratin-8- and -18-positive LE cells and smooth muscle α-actin (SMA)- and keratin-14-positive ME cells (Gudjonsson et al., 2005). In adult mammary glands, SMA-positive (SMA+) cells are basally located and generally align with the long axis of quiescent ducts. However, during pubertal branching morphogenesis, SMA+ cells adopt a characteristic stellate morphology (Figures S2A–S2D). These two different morphologies can coexist in adjacent regions of the same duct and imply a change in the behavior of SMA+ cells.

To visualize ME behavior during branching morphogenesis, we utilized a reporter mouse in which the keratin-14 promoter drives expression of an actin-EGFP fusion protein (K14-GFP-actin; Vaezi et al., 2002). K14-GFP-actin cells in the intact mammary gland were also SMA+ (Figure S2E) and basally located. Based on these markers, we refer to K14-GFP-actin+ or SMA + cells as ME cells and K14-GFP-actin− or SMA− epithelial cells as LE cells.

Luminal Clearance and Luminal Filling Precede Ductal Initiation

To determine the relative contributions of ME cells and LE cells to mammary branching morphogenesis, we stained all cells with CellTracker Red and then collected a series of 134 long-term confocal movies of organoids from K14-GFP-actin mice. The organoids began as multilayered epithelia and progressively resolved into bilayered structures with large, clear lumens and a single, complete basal ME layer (Figures 1F and 1F′; Movie S2). Once the lumens were cleared, the organoids filled their lumens again, predominately with LE cells (Figures 1G and 1G′; Movie S3). We termed this solid structure a “complex cyst” (Figures 1I–1L).

Complex cysts had a single basal ME layer and multiple LE layers, but they also had rare internal SMA+ cells (Figure 1I), similar to the basal-type body cells in TEBs (Mailleux et al., 2007). Epithelial polarity was also reduced, with atypical protein kinase C-ζ (APKC-ζ and β-catenin (Figures 1J and 1K) present at essentially all sites of cell-cell contact, instead of being restricted into distinct apical and basolateral domains. Complex cysts still retained polarity at a tissue level, however, with apically localized zona occludens 1 (ZO-1) marking luminal surfaces and basally localized β1-integrin marking the cell-matrix border and some sites of cell-cell contact (Figure 1L). The complex cyst stage in culture more closely resembled the TEB in vivo than the quiescent duct (Figure S1). This transition from a multilayered epithelium to a bilayered epithelium and back to a multilayered epithelium (Figures 1F and 1G) was characteristic of all organoids examined.

New Ducts Initiate from a Multilayered Epithelium

Ductal initiation from complex cysts was a transition from an essentially filled lumen to a progressively clearing lumen, with new ducts initiating and elongating at gaps in ME coverage (Figures 2A and 2B; Movies S4 and S5). The fronts of the elongating ducts were always multilayered, but there was often thinning and reversion to a bilayer at adjacent sites. LE cells appeared adherent to each other, yet they moved chaotically in the direction of elongation, whereas ME cells moved both toward and counter to the direction of ductal elongation.

Branching morphogenesis resulted from the interplay between ME and LE motility. We observed LE ducts elongate past ME coverage, followed by ME migration to restore coverage. We observed ME cells fully covering (Figure 2B′) or partially covering an elongating LE duct (Figure 2B″). Ducts typically stopped elongating after full coverage by ME cells, whereas ducts typically bifurcated after partial coverage by ME cells. We verified that the location of SMA + cells was similar to that of K14-GFP-actin+ cells, and we frequently observed SMA+ cells at sites of bifurcation (Figures 2C–2G). We could not distinguish whether ME cells induced bifurcations or responded to a separate decision to bifurcate, but ME motility closely correlated with changes in the shape of elongating ducts (Movie S5).

Cessation of elongation was accompanied by a transition in the tip of the duct from a multilayered epithelium to a single or bilayered epithelium, shown in an organoid derived from a transgenic reporter mouse with GFP expressed in both LE and ME (β-actin-EGFP; Figure 3A; Movie S6). The tips of ducts in growth-arrested organoids were often free of SMA+ cells (Figure 2G). The timing and extent of ductal elongation varied among organoids, but each eventually stopped elongating and reverted to a bilayered organization.

Cells within Elongating Ducts Migrate Collectively, but Remain Epithelial

Since the multilayered tips of elongating ducts were organized quite differently from quiescent ducts, we sought to determine if they remained epithelial during morphogenesis. On the basis of close cellular association and the consistent localization of E-cadherin and β-catenin to surfaces of intercellular contact throughout branching (Figures 3B, 3E, and 3F), we conclude that ducts remained epithelial. Epithelia also characteristically have basement membranes at their basal surface. We chose to stain for laminin 332, as it is a component of mammary epithelial basement membrane, but not of Matrigel. Unbranched structures, whether simple or complex cysts, displayed complete coverage with laminin 332 (Figure 3C), whereas the tips of actively elongating ducts were generally free of laminin 332 (Figure 3D). We could not distinguish whether laminin 332 was proteolytically degraded, displaced, or simply not synthesized at these sites.

During Collective Epithelial Migration, Cells Are Incompletely Polarized

To determine whether apicobasal polarity was retained during elongation, we used four molecular markers: β-catenin to mark basolateral cell surfaces, APKC-ζ to mark apical cell surfaces, β1-integrin to mark cell-matrix interactions, and ZO-1 to mark luminal surfaces.

At the cellular level, APKC-ζ and β-catenin were both detected at all lateral cell surfaces in the multilayered region during the complex cyst phase and during active elongation. APKC-ζ colocalized with ZO-1, whereas β-catenin was distinct from ZO-1. We conclude that cells in the multilayered region are incompletely polarized and do not have distinct apical and basolateral domains (Figures 3E–3H).

At the tissue level, we observed β1-integrin localized to the cell-matrix interface (Figures 3I and 3J) and sometimes also to lateral sites of cell-cell contact (Figure 3I, yellow). ZO-1 localized to luminal surfaces and to small pockets and channels within the multilayered region. We conclude that the multilayered epithelium is polarized at the tissue level, but its constituent cells are incompletely polarized relative to cells within quiescent regions of mammary epithelium.

Proliferation Is Required to Form Complex Cysts

Previous work showed that growth factor-induced proliferation is highest just before ductal initiation (Fata et al., 2007). We confirmed those results by staining for mitotic cells with phosphohistone H3 (H3-P) and observed frequent mitotic cells in the complex cyst and early branching stages (Figures 3K and 3L); there were fewer mitotic cells in simple cysts or late branching organoids. H3-P+ cells were present in all regions of organoids and showed no obvious correlation between the location of proliferation and the direction of extension.

Proliferation could be required to initiate branching, or to provide new cells to enlarge a branched structure. To distinguish whether inhibition of proliferation would produce arrest at the simple cyst stage or produce small, branched organoids, we inhibited DNA polymerase A by using aphidicolin. When added 24 or 48 hr into culture, aphidicolin completely blocked branching. At doses of 5 or 10 μM, all organoids arrested at the simple cyst stage (Figure S2); therefore, proliferation is required to form the multilayered, complex cyst.

Ductal Elongation Is Accomplished by a Multilayered Epithelium

We sought to determine the cellular mechanism of ductal initiation from complex cysts. To observe the cellular basis of ductal initiation, we collected 127 confocal time-lapse movies of initiating and elongating ducts. We observed that new ducts always initiated as multilayered epithelial structures (N = 394/394 ducts in 127 movies; Figure 4A′; Movies S4–S8). Significantly, we never observed basally directed protrusions, cell migration out of the luminal epithelium, or initiation and elongation of fully polarized epithelial ducts (N = 0/394 ducts), ruling out chain migration as the mechanism for tubulogenesis in this system. Instead, ductal elongation was accomplished by a collectively migrating, dynamically rearranging, multilayered epithelium at the ductal tip. This structure reverted to a bilayered epithelium surrounding a simple lumen in the trailing duct (Figure 4A′). The thinning of the trailing duct from multiple to a single luminal layer also contributed to ductal elongation.

Ductal Elongation Occurs without Leading Cellular Extensions

Leading cell extensions or specialized actin-rich protrusions, such as filopodia and lamellipodia, are typically observed at the leading edge of individual migratory cells (Mitchison and Cramer, 1996) and of collectively migrating groups of cells, ranging from *Drosophila* border cells (Fulga and Rorth, 2002; Prasad and Montell, 2007) to zebrafish neural precursors (Lecaudey and Gilmour, 2006). In contrast to these previous studies, we never

observed cellular extensions or actin-rich protrusions at the front of advancing mammary ducts (Figures 4B–4B‴, N > 250). Instead, F-actin was enriched along lateral cell surfaces and colocalized with ZO-1 at luminal surfaces.

Cells Dynamically Rearrange during Collective Epithelial Migration

We next asked if a constant group of cells remained at the invasion front or if cells exchanged positions during invasion (Figures 4C–4C″). To distinguish these possibilities, we followed individual cells during ductal extension by exploiting the mosaic expression of EGFP within the mammary epithelium of mice in which GFP was knocked into the Sca-1 locus (Sca-1-EGFP). To provide context, all cells were stained with CellTracker Red.

Cells in the multilayered region of the extending duct continuously exchanged positions (N = 394 ducts in 127 movies; see Movies S7 and S8). This cell rearrangement was characteristic of both newly initiated ducts (Figures 2A and 2B) and later ducts with well-defined lumens (Figures 3A, 4A′, and 4C′). We verified this conclusion by using three different GFP reporter lines: K14-GFP-actin (Figures 2A and 2B), Sca-1-EGFP (Figures 4A′ and 4C′), and β-actin-EGFP transgenic mice (Figure 3A). In all cases, the cells at the tip of the extending ducts dynamically rearranged.

Duct Initiation Requires Rac-1 and Myosin Light Chain Kinase

What are the molecular regulators of ductal initiation? Previous studies in mammary epithelium (Vargo-Gogola et al., 2006), ureteric bud (Meyer et al., 2006), 3D MDCK morphogenesis (Yu et al., 2003), and epidermis (Vaezi et al., 2002) identified Rac- and Rho-type GTPases as critical regulators of epithelial morphogenesis. Accordingly, we tested the role of these pathways in mammary epithelial branching morphogenesis, by using soluble inhibitors: Rac-1 Inhibitor (NSC23766) for Rac, Y27632 for Rho kinase (ROCK), and ML7 for myosin light chain kinase (MLCK).

Rac inhibition resulted in a strong dose-dependent inhibition of ductal initiation (Figure 5A). Rac-inhibited cysts were covered externally by ME cells, but they also had convoluted internal tubules, with associated internal ME cells (Figure 5D) and differed markedly from the normal complex cysts (Figures 1I–1K). These internal tubules were not observed in control organoids (Figure 5C). Movies of organoids from the K14-GFP-actin (Figure 5G; Movie S9; 24 movies total) or β-actin-EGFP (not shown) transgenic mice revealed that the cysts were relatively static and had extensive ME coverage, internal ME cells, and persistently filled lumens.

MLCK inhibition also prevented ductal initiation in a dose-dependent fashion (Figures 5B, 5E, and 5F). Maximal inhibition was achieved at doses ranging from 4 to 10 μM, depending on the experiment. We did not observe internal tubules in MLCK-inhibited cysts. Long-term confocal movies of K14-GFP-actin organoids (Figure 5H; Movie S10) and β-actin-EGFP organoids (not shown) revealed that MLCK-inhibited organoids transiently formed complex cysts, but then gradually cleared their lumens and restored a largely bilayered epithelial structure (19 movies total). MLCK-inhibited organoids remained persistently enclosed in ME cells.

ROCK Is Required to Restore Bilayered Epithelial Architecture

As ducts ceased elongating, they transitioned from a multilayered epithelium to a single luminal layer (Figure 3A). We sought to understand the molecular regulation of this transition. Recent work identified p190-B Rho-GTPase as a regulator of mammary epithelial architecture, with its inactivation resulting in hyperplasia and disorganized myoepithelial coverage (Vargo-Gogola et al., 2006). Accordingly, we used Y-27632 (Uehata et al., 1997) to inhibit the related molecules ROCK1 and ROCK2. ROCK inhibitor-treated organoids branched at equal or higher

rates than controls, but they were heterogeneous and poorly patterned (Figure 6; Figure S3; Movies S12 and S14–S17). The effects were acutely reversible when ROCK inhibitor was washed out (Figure S3E; Movie S17).

Our data indicate that ME location, behavior, and migration reflect, and appear to influence, the pattern of branching morphogenesis (Figures 1 and 2). ROCK inhibition resulted in disorganized, incomplete coverage by ME cells. After ROCK inhibition, ME cells were often spindle shaped, with no obvious correlation between ME position and final organoid structure (Figures 6B and 6C).

In control organoids, there was a sharp organizational difference between the multilayered, elongating end and the trailing duct behind it (Figure 4A′). The trailing ducts of control organoids had clear, ZO-1-lined lumens, apically enriched F-actin, and a simple, bilayered structure. ROCK-inhibited organoids had no central lumen and instead localized ZO-1 and F-actin to small foci and had a persistent, disorganized, multilayered structure. No ROCK inhibitor-treated organoids were observed to revert to a bilayered architecture. LE cell shapes were also rounder, but E-cadherin remained localized to lateral LE surfaces in ROCK inhibitor-treated organoids, suggesting that the cells remained adherent and epithelial (Figure 6G). ROCK-inhibited organoids had abnormally positioned ME cells, abnormal LE and ME cells shapes, no central lumens, and a persistent failure to revert from a multilayered to a bilayered architecture.

To characterize the kinetics and cell behavioral basis of the ROCK inhibitor phenotype, we collected 67 long-term confocal movies from K14-GFP-actin (Figure 6M; Movie S12), β-actin-EGFP (Figure S3C; Movie S15), and Sca-1-EGFP (Figure S3D; Movie S16). The effect of ROCK inhibition was acute, with changes in ME coverage and LE organization observable within 12 hr. A major question was the degree to which the abnormal architecture of the LE related to the loss of ME coverage (Figures 6B and 6C).

ME cells appear to play a restraining role in normal organoids and seem to limit and pattern LE mobility (Figures 2A–2B″; Movies S4 and S5). We examined the acute effects of ROCK inhibition on ME behavior by filming in parallel control and ROCK inhibitor-treated organoids from the same K14-GFP-actin+ mouse 1 hr after ROCK inhibition (Figures 6L and 6M; Movies S11 and S12). In control organoids, ducts initiated through gaps in ME coverage, elongated through the combined motility of LE cells and ME cells, and reverted to a bilayered architecture. Conversely, in ROCK-inhibited organoids, ME cells quickly changed shape, and their motility had little relationship to the vigorous growth of the largely LE organoid.

We next sought to distinguish whether LE behavior was altered in ROCK-inhibited organoids, by using GFP reporters that highlighted LE behavior. In control organoids, LE cells rearrange vigorously in the multilayered ends of ducts, but they are more restrained in the trailing duct region (Figure 4). In ROCK-inhibited organoids, LE cells rearranged vigorously throughout the multilayered epithelium (Sca-1-EGFP, Figure S3D; Movie S16; β-actin-EGFP, Figure S3; Movie S15). Taken together, these findings demonstrate that ROCK inhibition induces acute changes in LE and ME cell shape and cell behavior, abnormal epithelial architecture, and collapse of the lumen. ROCK inhibition results in a hyperbranched epithelium with disorganized ME coverage and prevents restoration of bilayered epithelial architecture.

Normal and Neoplastic Mammary Epithelial Morphogenesis In Vivo Occurs via a Multilayered Epithelial State

Does the multilayered epithelium we observe in culture resemble the in vivo epithelial organization of mammary ducts during morphogenesis? We selected two examples of in vivo epithelial morphogenesis: (1) TEBs during normal pubertal morphogenesis and (2)

hyperplasias from a pathologically validated mouse model of luminal-type breast cancer (Herschkowitz et al., 2007; Lin et al., 2003), in which polyoma virus middle T oncogene is expressed under the control of the mouse mammary tumor virus promoter (MMTV-PymT) (Guy et al., 1992).

We first compared TEBs and quiescent ducts during normal morphogenesis in vivo to the multilayered epithelial organization of elongating ducts in culture (Figure S1). TEBs were multilayered and were enclosed in a layer of SMA+ cap cells. In the multilayered body cell region of TEBs, β-catenin, APKC-ζ, and β1-integrin all localized to lateral cell surfaces. ZO-1 localized apically, but largely to finger-like projections and isolated pockets within the multilayered body cell region. The lumens of quiescent ducts in vivo were simple and were lined by a single luminal epithelial layer, with apically localized ZO-1 and APKC-ζ, basolaterally localized β-catenin, and basally localized β1-integrin. TEBs were also hyperproliferative relative to quiescent ducts. The most notable differences between TEBs in vivo and elongating ducts of organoids in culture were that TEBs were composed of significantly more cells and encountered a much more diverse cellular stroma. Therefore, the epithelial organization of TEBs in vivo and elongating ducts in culture was similar.

In early MMTV-PymT hyperplasias, we observed a progressive loss of SMA+ ME cells, with fewer ME cells correlating with less normal ductal morphology (Figure 7A), consistent with previous reports (Lin et al., 2003). Regions with little or no ME coverage were always multilayered. ZO-1 in multilayered hyperplasias was localized in small pockets (Figures 7A and 7B). In later lesions, SMA+ cells were rare or absent. In multilayered hyperplasias, β-catenin localized to all sites of cell-cell contact, indicating incomplete apicobasal polarity (Figure 7B). Therefore, normal and neoplastic epithelia during morphogenesis share a similar multilayered epithelial organization (Figures 7A–7D).

Discussion

Our study has provided new insights into mammary branching morphogenesis and has identified a different type of collective epithelial migration without leading cellular extensions or protrusions. We dissected the process of branching morphogenesis into discrete subprocesses by using time-lapse confocal microscopy, and we identified molecular pathways regulating each subprocess (Figure 7). We showed that mammary epithelium first reorganizes from a quiescent, bilayered epithelium to a preinvasive, highly proliferative, incompletely polarized, multilayered epithelium. We identified Rac and MLCK as molecular regulators of the transition from this preinvasive state to the initiation of new ducts. We observed that cells within extending ducts dynamically rearrange, but remain adherent and localize E-cadherin and β-catenin to cell-cell contacts. During this collective epithelial migration, the tissue has distinct luminal- and basement membrane-contacting surfaces, but individual cells within the multilayered region are incompletely polarized. Finally, ROCK signaling is required to restore simple, bilayered epithelial architecture.

Models of Collective Cell Movement

Recent time-lapse imaging studies have established models for the collective movement of groups of cells, including neuronal precursors in the zebrafish lateral line (Lecaudey and Gilmour, 2006), epithelial cells during *Drosophila* dorsal closure (Jacinto et al., 2000), and border cell migration in *Drosophila* (Bianco et al., 2007; Prasad and Montell, 2007). In each of these examples, cells at the front of the migrating group extended cellular extensions or protrusions in the direction of movement. By contrast, cells at the front of elongating mammary ducts did not have leading cellular extensions or actin-rich protrusions. As protrusive activity can function to guide cells, how elongating mammary ducts move directionally remains an open question.

The Role of Myoepithelial Cells in Branching Morphogenesis

ME cells are implicated in normal development and neoplastic progression in the mammary gland (Gudjonsson et al., 2005; Polyak and Hu, 2005) and have been identified as cellular tumor suppressors (Sternlicht et al., 1997). However, because most cell culture models of mammary morphogenesis contain only one cell type, often of mixed myoepithelial and luminal character, ME function has often been overlooked.

We directly monitored ME cell behavior during branching morphogenesis and observed ductal initiation at breaks in ME coverage, active migration of ME cells over the surface of LE in ducts, and a close relationship between ME localization, ME motility, and the resulting pattern of branching morphogenesis. In time-lapse movies, ME migration precede bifurcations. However, our results do not formally distinguish whether ME cells actively regulate ductal initiation and patterning or are early responders to another signal. In each of our perturbations, the localization of ME cells marked the resulting phenotype. Rac or MLCK inhibition blocked duct initiation and resulted in cysts with extensive ME coverage. ROCK inhibition resulted in a disorganized hyperbranching phenotype and disorganized, incomplete ME coverage. Our results suggest an important role for ME cells as cellular regulators of tissue architecture.

Do other branched epithelial organs rely on a similar balance between different cell types to produce branched ductal networks? Recent work in the vascular system has shown that perivascular smooth muscle cells or pericytes influence the patterning and function of endothelial networks in normal development and cancer (Hall, 2006; Song et al., 2005).

Epithelial Morphogenesis during Development

We demonstrated that epithelial architecture and polarity can be dramatically regulated in time and space within a group of actively rearranging cells. Our study followed live mammary epithelial cells through a reversible conversion from a highly polarized bilayered organization to a low-polarity, multilayered intermediate. Our observations build on genetic studies identifying cell adhesion proteins as critical regulators of mammary development and breast cancer (Hinck and Silberstein, 2005; Katz and Streuli, 2007; Knudsen and Wheelock, 2005).

Most work on epithelial morphogenesis has focused on embryonic tissues (e.g., lung [Liu et al., 2004], ureteric bud [Costantini, 2006; Meyer et al., 2004; Pohl et al., 2000], and salivary gland [Patel et al., 2006]) or immortalized cell lines such as MDCK cells (Zegers et al., 2003). Active cell rearrangements within a multilayered epithelium have been noted during embryonic branching morphogenesis of the salivary gland in organ culture, but these movements declined with age and were not observed in neonatal tissue (Larsen et al., 2006).

Although the polarity of mature epithelia is well understood and recent work has illuminated how polarity emerges after initial cell-cell contact (Nejsum and Nelson, 2007; Yeaman et al., 1999), less attention has been paid to changes in apicobasal polarity during morphogenesis and tissue remodeling in adult tissues. Intriguingly, apicobasal polarity is also downmodulated during morphogenesis in other systems, including embryonic neurectoderm (Aaku-Saraste et al., 1996; Lee et al., 2007) and HGF-induced tubulogenesis in 3D MDCK cultures (Zegers et al., 2003).

We propose that the properties of stable epithelial polarity, distinct apicobasal membrane domains, and a single luminal cell layer used to define simple epithelia might instead be characteristic only of morphogenetically inactive epithelia. It is of interest to determine whether all vertebrate epithelial tissues must enter into an incompletely polarized, multilayered intermediate to remodel or repair their structure as well as what signaling pathways regulate entry into and exit from the multilayered state.

The Morphogenetically Active Epithelial State

We suggest that this reversible conversion of epithelial organization represents a regulated transition between different states of the same epithelium, rather than a transformation of epithelial type (metaplasia). As such, the shared low-adhesion, low-polarity, multilayered epithelial state that we observe in normal and neoplastic epithelium during morphogenesis may be an epithelial state specialized to allow growth and remodeling of the epithelium. We suggest the term "morphogenetically active epithelial state" to describe the organizational state of mammary epithelium during morphogenesis. We hypothesize that similar transitions between different states of epithelial organization may be a general developmental mechanism for remodeling and repairing epithelial tissues.

Alternate Strategies for Collective Cell Movement

Collective epithelial migration lacks many of the features classically associated with an invasive or migratory phenotype, such as forward-oriented, cellular extensions or actin-rich protrusions (Mitchison and Cramer, 1996). It has been noted in clinical specimens and in explanted human 3D cultures that tumors can invade singly or as connected groups of cells (Friedl et al., 2004; Hegerfeldt et al., 2002). Clearly, there is more than one possible underlying cellular mechanism for tissue invasion, and additional work is needed to determine the relative importance of collective epithelial migration versus classic protrusive invasion in human tissue repair and in diseases such as breast cancer. It is also of critical importance to determine whether the cellular mechanisms of tissue invasion are cell type specific, or whether cellular invasion mechanisms may depend on the interplay between cell intrinsic factors and tissue microenvironmental context.

Epithelial Morphogenesis during Cancer Progression

We propose that a primary defect in early cancerous lesions may be aberrant entry into, or persistence in, a fundamentally normal "morphogenetically active epithelial state" (Figure 7F). To test the limits of this model, it will be important to make careful comparisons between three states: normal quiescent epithelium, normal morphogenetically active epithelium, and neoplastic morphogenetically active epithelium. Our results support the concept that early stages of cancer progression may result from fundamentally normal processes occurring at the wrong time and place.

Experimental Procedures

GFP Reporter Lines

Animal experiments were approved by the Institutional Animal Care and Use Committee (IACUC) at University of California, San Francisco. We used transgenic mice in which a GFP-actin fusion protein was expressed under the control of the keratin-14 promoter (K14-GFP-actin), acquired from E. Fuchs, Rockefeller University (Vaezi et al., 2002). The second mouse model expressed EGFP, knocked into the Sca-1 locus (Sca-1-EGFP), mosaically throughout the mammary epithelium (provided by T. Graubert, Washington University; Hanson et al., 2003). Transgenic mice expressing EGFP under the control of the β-actin promoter (β-actin-EGFP; Hadjantonakis et al., 1998) were obtained from Jackson Laboratory. FVB/N mice were purchased from Charles River.

Isolation of Primary Mammary Organoids

Cultures were prepared as previously described (Fata et al., 2007). Briefly, glands were minced and tissue was shaken for 30 min at 37°C in a 50 ml collagenase/trypsin solution in DMEM/F12 (GIBCO-BRL), 0.1 g trypsin (GIBCO-BRL), 0.1 g collagenase (Sigma C5138), 5 ml fetal calf serum, 250 μl of 1 μg/ml insulin, and 50 μl of 50 μg/ml gentamicin (all University of

California, San Francisco Cell Culture Facility). The collagenase solution was centrifuged at 1500 rpm for 10 min, dispersed through 10 ml DMEM/F12, centrifuged at 1500 rpm for 10 min, and then resuspended in 4 ml DMEM/F12 + 40 μl DNase (2U/μl) (Sigma). The DNase solution was shaken by hand for 2–5 min, then centrifuged at 1500 rpm for 10 min. Organoids were separated from single cells through four differential centrifugations (pulse to 1500 rpm in 10 ml DMEM/F12). The final pellet was resuspended in the desired amount of Growth Factor Reduced Matrigel (BD Biosciences).

Organoid Assay

Organoid assays were performed in 24-well coverslip bottom plates (E&K Scientific EK-42892) for confocal time-lapse imaging and in 4-well coverslip bottom chambers (Nunc 155383) for routine culture. Typically, a 50 μl suspension of organoids in Matrigel was added to each well, followed by 30 min at 37°C. We then added minimal media (DMEM/F12, 1% v/v insulin, transferrin, selenium [Sigma] and 1% v/v penicillin/streptomycin [100× stock]) or FGF2/branching medium (minimal medium + 2.5 nM FGF2 [Sigma F0291]). Inhibitors were used in a minimum of three separate experiments with similar results. Representative single experiments are shown. ROCK inhibitor (Y27632; Chemicon), Rac-1 inhibitor (NSC23766, Calbiochem), ML-7 (Calbiochem), and aphidicolin (Sigma) were used as indicated. All inhibitor experiments discussed in the text were done in FGF2 medium. ROCK inhibitor treatment in minimal medium resulted in simple cysts, which were indistinguishable from control organoids.

Antibody Staining

Organoids were equilibrated in 25% sucrose in PBS for 1 hr, fixed in cold 1:1 methanol:acetone overnight at −20°C, then re-equilibrated in 25% sucrose in PBS for 1 hr. Samples were blocked for 1 hr with 5% serum, incubated with primary antibody (all 1:250 in PBS) for 2 hr to overnight, and rinsed three times in PBS. Secondary antibodies (Molecular Probes Alexa series, all 1:250 in PBS) were incubated with the organoids for 1–4 hr. F-actin was stained with Alexa 488 or 568 Phalloidin (1:40–1:100), and nuclei were stained with To-Pro-3, DAPI, or propidium iodide (all 1:1000) (Molecular Probes). Antibody stains were done at least 3 independent times, and a minimum of 25 organoids were inspected in each condition each time. Primary antibodies were E-cadherin (Zymed, 13-1900), ZO-1 (Chemicon, MAB1520), SMA (Sigma, F3777 or C6198), APKC-ζ (Santa Cruz, sc-216), β-catenin (Santa Cruz, sc-7199), phospho-histone H3 (Santa Cruz, sc-8656-R), β1-integrin (BD PharMingen, 553715), and rabbit anti-laminin 332 (gift of Peter Marinkovich, Stanford University, and Monique Aumailley, University of Cologne, Germany).

Time-Lapse Microscopy

Bright-field time-lapse movies were collected on a Zeiss Axiovert S-100 microscope by using a 10× A-Plan objective lens, a Ludl shutter, a Cohu CCD camera, and a Ludl x-y-z motorized stage. Temperature was held at 37°C and CO_2 was held at 5% by using a CTI Controller 3700 and Temperature Control 37.2 combination. Images were acquired at 24 positions every 15 min by using OpenLab 4.0.2. (Improvision, Inc.).

Confocal movies and antibody-stained samples were imaged on a custom-built spinning disk confocal microscope (Solamere Technology Group, Salt Lake City, UT). Briefly, the system includes a Carl Zeiss Axiovert 200M microscope, a Yokogawa CSU-10 confocal, an Applied Scientific Instruments (ASI) MS-2000 motorized stage, an ASI FW-1000 filter wheel, Dynamic Lasers argon and krypton lasers, and a Blue Sky 405 laser. Objective lenses used were Zeiss 10× Fluar, 20× Fluar, 20× LD-Plan Neofluar, 40× LD-Plan Neofluar, and 40× C-Apochromat. Time-lapse movies ranged in length from 20–105 hr, and images were collected every 10–15 min; 5–50 movies were collected in parallel. Images were collected by using QED

In Vivo (Media Cybernetics) and were analyzed by using Imaris (Bitplane). Environmental control was achieved through a home-built heater box (Kulesa and Fraser, 1999) and a World Precision Instruments Air Therm ATX. CellTracker Red (Molecular Probes) was used at 1–10 μM, and cells were stained for 1–10 hr. Optimal staining was achieved at 24 hr of culture with 2 hr of staining with 1 μM CellTracker Red, followed by three rinses of 15 min each.

Image Processing

Levels on images were adjusted in Adobe Photoshop to match the collected intensity histogram to the full 8 bit output range.

Supplementary Material

Refer to Web version on PubMed Central for supplementary material.

Acknowledgments

This study was supported by National Institutes of Health (NIH) grants to Z.W. (CA057621 and ES012801) and postdoctoral fellowships to A.J.E. (NIH National Research Service Award [HL-007731] and California Breast Cancer Research Program [11FB-0015]). We thank John Wallingford and Keith Mostov for critical comments on the manuscript; Mina Bissell, Jimmie Fata, Mark Sternlicht, Mikala Egeblad, and Joanna Phillips for stimulating discussions of the data; and Marina Burkova, Ying Yu, and Helen Capili for technical assistance. We thank Nicole Stokes and Elaine Fuchs for the K14-GFP-actin mouse line; M. Peter Marinkovich and Monique Aumailley for the laminin-332 antibodies; and George Peeters, Gary Rondeau, John Zemek, Mike Buchin, Lee Pochop, Ciprian Almonte, Bob Cowden, and Kevin Frischmann for microscopy support.

References

Aaku-Saraste E, Hellwig A, Huttner WB. Loss of occludin and functional tight junctions, but not ZO-1, during neural tube closure–remodeling of the neuroepithelium prior to neurogenesis. Dev Biol 1996;180:664–679. [PubMed: 8954735]

Bianco A, Poukkula M, Cliffe A, Mathieu J, Luque CM, Fulga TA, Rorth P. Two distinct modes of guidance signalling during collective migration of border cells. Nature 2007;448:362–365. [PubMed: 17637670]

Bilder D. Epithelial polarity and proliferation control: links from the *Drosophila* neoplastic tumor suppressors. Genes Dev 2004;18:1909–1925. [PubMed: 15314019]

Costantini F. Renal branching morphogenesis: concepts, questions, and recent advances. Differentiation 2006;74:402–421. [PubMed: 16916378]

Fata JE, Mori H, Ewald AJ, Zhang H, Yao E, Werb Z, Bissell MJ. The MAPK(ERK-1,2) pathway integrates distinct and antagonistic signals from TGFα and FGF7 in morphogenesis of mouse mammary epithelium. Dev Biol 2007;306:193–207. [PubMed: 17448457]

Friedl P, Hegerfeldt Y, Tusch M. Collective cell migration in morphogenesis and cancer. Int J Dev Biol 2004;48:441–449. [PubMed: 15349818]

Fulga TA, Rorth P. Invasive cell migration is initiated by guided growth of long cellular extensions. Nat Cell Biol 2002;4:715–719. [PubMed: 12198500]

Gudjonsson T, Adriance MC, Sternlicht MD, Petersen OW, Bissell MJ. Myoepithelial cells: their origin and function in breast morphogenesis and neoplasia. J Mammary Gland Biol Neoplasia 2005;10:261–272. [PubMed: 16807805]

Guy CT, Cardiff RD, Muller WJ. Induction of mammary tumors by expression of polyomavirus middle T oncogene: a transgenic mouse model for metastatic disease. Mol Cell Biol 1992;12:954–961. [PubMed: 1312220]

Hadjantonakis AK, Gertsenstein M, Ikawa M, Okabe M, Nagy A. Generating green fluorescent mice by germline transmission of green fluorescent ES cells. Mech Dev 1998;76:79–90. [PubMed: 9867352]

Hall AP. Review of the pericyte during angiogenesis and its role in cancer and diabetic retinopathy. Toxicol Pathol 2006;34:763–775. [PubMed: 17162534]

Hanson P, Mathews V, Marrus SH, Graubert TA. Enhanced green fluorescent protein targeted to the Sca-1 (Ly-6A) locus in transgenic mice results in efficient marking of hematopoietic stem cells in vivo. Exp Hematol 2003;31:159–167. [PubMed: 12591281]

Hegerfeldt Y, Tusch M, Brocker EB, Friedl P. Collective cell movement in primary melanoma explants: plasticity of cell-cell interaction, β1-integrin function, and migration strategies. Cancer Res 2002;62:2125–2130. [PubMed: 11929834]

Hennighausen L, Robinson GW. Information networks in the mammary gland. Nat Rev Mol Cell Biol 2005;6:715–725. [PubMed: 16231422]

Herschkowitz JI, Simin K, Weigman VJ, Mikaelian I, Usary J, Hu Z, Rasmussen KE, Jones LP, Assefnia S, Chandrasekharan S, et al. Identification of conserved gene expression features between murine mammary carcinoma models and human breast tumors. Genome Biol 2007;8:R76. [PubMed: 17493263]

Hinck L, Silberstein GB. Key stages in mammary gland development: the mammary end bud as a motile organ. Breast Cancer Res 2005;7:245–251. [PubMed: 16280048]

Howlin J, McBryan J, Martin F. Pubertal mammary gland development: insights from mouse models. J Mammary Gland Biol Neoplasia 2006;11:283–297. [PubMed: 17089203]

Jacinto A, Wood W, Balayo T, Turmaine M, Martinez-Arias A, Martin P. Dynamic actin-based epithelial adhesion and cell matching during *Drosophila* dorsal closure. Curr Biol 2000;10:1420–1426. [PubMed: 11102803]

Katz E, Streuli CH. The extracellular matrix as an adhesion checkpoint for mammary epithelial function. Int J Biochem Cell Biol 2007;39:715–726. [PubMed: 17251051]

Knudsen KA, Wheelock MJ. Cadherins and the mammary gland. J Cell Biochem 2005;95:488–496. [PubMed: 15838893]

Kulesa PM, Fraser SE. Confocal imaging of living cells in intact embryos. Methods Mol Biol 1999;122:205–222. [PubMed: 10231794]

Larsen M, Wei C, Yamada KM. Cell and fibronectin dynamics during branching morphogenesis. J Cell Sci 2006;119:3376–3384. [PubMed: 16882689]

Lecaudey V, Gilmour D. Organizing moving groups during morphogenesis. Curr Opin Cell Biol 2006;18:102–107. [PubMed: 16352429]

Lee C, Scherr HM, Wallingford JB. Shroom family proteins regulate {γ}-tubulin distribution and microtubule architecture during epithelial cell shape change. Development 2007;134:1431–1441. [PubMed: 17329357]

Lin EY, Jones JG, Li P, Zhu L, Whitney KD, Muller WJ, Pollard JW. Progression to malignancy in the polyoma middle T oncoprotein mouse breast cancer model provides a reliable model for human diseases. Am J Pathol 2003;163:2113–2126. [PubMed: 14578209]

Liu Y, Stein E, Oliver T, Li Y, Brunken WJ, Koch M, Tessier-Lavigne M, Hogan BL. Novel role for Netrins in regulating epithelial behavior during lung branching morphogenesis. Curr Biol 2004;14:897–905. [PubMed: 15186747]

Mailleux AA, Overholtzer M, Schmelzle T, Bouillet P, Strasser A, Brugge JS. BIM regulates apoptosis during mammary ductal morphogenesis, and its absence reveals alternative cell death mechanisms. Dev Cell 2007;12:221–234. [PubMed: 17276340]

Meyer TN, Schwesinger C, Bush KT, Stuart RO, Rose DW, Shah MM, Vaughn DA, Steer DL, Nigam SK. Spatiotemporal regulation of morphogenetic molecules during in vitro branching of the isolated ureteric bud: toward a model of branching through budding in the developing kidney. Dev Biol 2004;275:44–67. [PubMed: 15464572]

Meyer TN, Schwesinger C, Sampogna RV, Vaughn DA, Stuart RO, Steer DL, Bush KT, Nigam SK. Rho kinase acts at separate steps in ureteric bud and metanephric mesenchyme morphogenesis during kidney development. Differentiation 2006;74:638–647. [PubMed: 17177859]

Mitchison TJ, Cramer LP. Actin-based cell motility and cell locomotion. Cell 1996;84:371–379. [PubMed: 8608590]

Nejsum LN, Nelson WJ. A molecular mechanism directly linking E-cadherin adhesion to initiation of epithelial cell surface polarity. J Cell Biol 2007;178:323–335. [PubMed: 17635938]

Patel VN, Rebustini IT, Hoffman MP. Salivary gland branching morphogenesis. Differentiation 2006;74:349–364. [PubMed: 16916374]

Pilot F, Lecuit T. Compartmentalized morphogenesis in epithelia: from cell to tissue shape. Dev Dyn 2005;232:685–694. [PubMed: 15712202]

Pohl M, Stuart RO, Sakurai H, Nigam SK. Branching morphogenesis during kidney development. Annu Rev Physiol 2000;62:595–620. [PubMed: 10845104]

Polyak K, Hu M. Do myoepithelial cells hold the key for breast tumor progression? J Mammary Gland Biol Neoplasia 2005;10:231–247. [PubMed: 16807803]

Prasad M, Montell DJ. Cellular and molecular mechanisms of border cell migration analyzed using time-lapse live-cell imaging. Dev Cell 2007;12:997–1005. [PubMed: 17543870]

Simian M, Hirai Y, Navre M, Werb Z, Lochter A, Bissell MJ. The interplay of matrix metalloproteinases, morphogens and growth factors is necessary for branching of mammary epithelial cells. Development 2001;128:3117–3131. [PubMed: 11688561]

Song S, Ewald AJ, Stallcup W, Werb Z, Bergers G. PDGFRβ+ perivascular progenitor cells in tumours regulate pericyte differentiation and vascular survival. Nat Cell Biol 2005;7:870–879. [PubMed: 16113679]

Sternlicht MD. Key stages in mammary gland development: the cues that regulate ductal branching morphogenesis. Breast Cancer Res 2006;8:201. [PubMed: 16524451]

Sternlicht MD, Kedeshian P, Shao ZM, Safarians S, Barsky SH. The human myoepithelial cell is a natural tumor suppressor. Clin Cancer Res 1997;3:1949–1958. [PubMed: 9815584]

Sternlicht MD, Sunnarborg SW, Kouros-Mehr H, Yu Y, Lee DC, Werb Z. Mammary ductal morphogenesis requires paracrine activation of stromal EGFR via ADAM17-dependent shedding of epithelial amphiregulin. Development 2005;132:3923–3933. [PubMed: 16079154]

Uehata M, Ishizaki T, Satoh H, Ono T, Kawahara T, Morishita T, Tamakawa H, Yamagami K, Inui J, Maekawa M, Narumiya S. Calcium sensitization of smooth muscle mediated by a Rho-associated protein kinase in hypertension. Nature 1997;389:990–994. [PubMed: 9353125]

Vaezi A, Bauer C, Vasioukhin V, Fuchs E. Actin cable dynamics and Rho/Rock orchestrate a polarized cytoskeletal architecture in the early steps of assembling a stratified epithelium. Dev Cell 2002;3:367–381. [PubMed: 12361600]

Vargo-Gogola T, Heckman BM, Gunther EJ, Chodosh LA, Rosen JM. P190-B Rho GTPase-activating protein overexpression disrupts ductal morphogenesis and induces hyperplastic lesions in the developing mammary gland. Mol Endocrinol 2006;20:1391–1405. [PubMed: 16469769]

Williams JM, Daniel CW. Mammary ductal elongation: differentiation of myoepithelium and basal lamina during branching morphogenesis. Dev Biol 1983;97:274–290. [PubMed: 6852366]

Wiseman BS, Sternlicht MD, Lund LR, Alexander CM, Mott J, Bissell MJ, Soloway P, Itohara S, Werb Z. Site-specific inductive and inhibitory activities of MMP-2 and MMP-3 orchestrate mammary gland branching morphogenesis. J Cell Biol 2003;162:1123–1133. [PubMed: 12975354]

Woodward WA, Chen MS, Behbod F, Rosen JM. On mammary stem cells. J Cell Sci 2005;118:3585–3594. [PubMed: 16105882]

Yeaman C, Grindstaff KK, Nelson WJ. New perspectives on mechanisms involved in generating epithelial cell polarity. Physiol Rev 1999;79:73–98. [PubMed: 9922368]

Yu W, O'Brien LE, Wang F, Bourne H, Mostov KE, Zegers MM. Hepatocyte growth factor switches orientation of polarity and mode of movement during morphogenesis of multicellular epithelial structures. Mol Biol Cell 2003;14:748–763. [PubMed: 12589067]

Zegers MM, O'Brien LE, Yu W, Datta A, Mostov KE. Epithelial polarity and tubulogenesis in vitro. Trends Cell Biol 2003;13:169–176. [PubMed: 12667754]

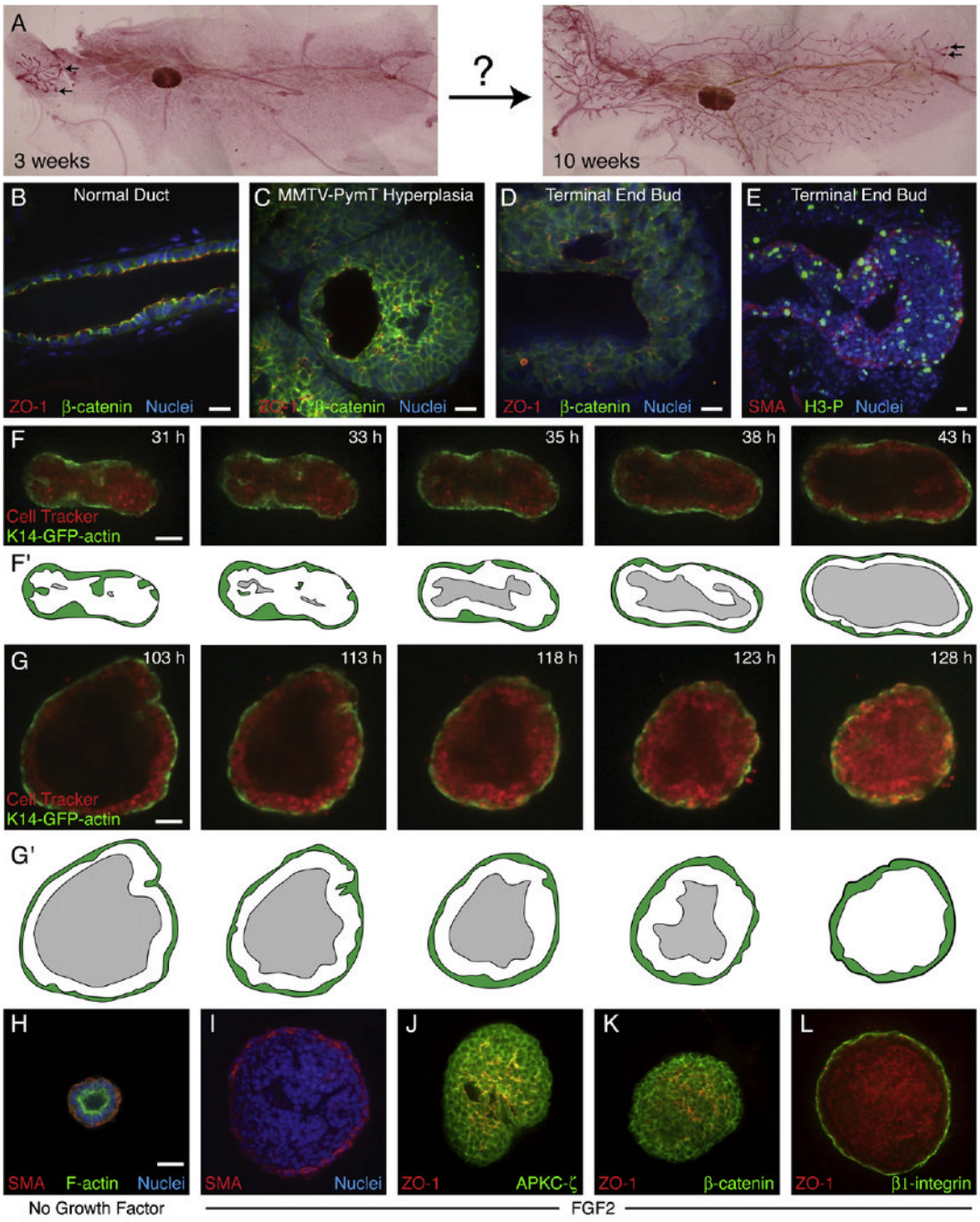

Figure 1. Mammary Epithelia Enter a Multilayered Epithelial State during Morphogenesis

(A) Mouse mammary ducts elongate greatly during puberty (carmine red-stained whole mounts). Terminal end buds (TEBs) are indicated (black arrows).

(B–E) Staining for zona occludens 1 (ZO-1), β-catenin, and nuclei (DAPI) in (B) a quiescent mammary duct, (C) a hyperplasia from a 14-week-old MMTV-PymT mouse, and (D) a TEB from a pubertal mouse. (E) A TEB from a pubertal mouse stained with smooth muscle actin (SMA) to indicate myoepithelial (ME) cells and phospho-histone H3 (H3-P) to indicate cells in mitosis.

(F and G) Single-section frames from a time-lapse movie showing (F) luminal clearance (Movie S2) and (G) luminal filling (Movie S3) in two different FGF2-treated, K14-GFP-actin/CellTracker Red-labeled organoids.
(F′ and G′) Schematic view of (F) and (G), respectively; the ME is green, and the lumen is gray.
(H) A simple, bilayered cyst, grown in minimal medium.
(I) A complex multilayered cyst, grown in FGF2 medium, with basally located SMA+ ME and internal SMA+ cells.
(J and K) In FGF2-treated complex cysts, (J) APKC-ζ and (K) β-catenin localize to all lateral cell surfaces, whereas ZO-1 localizes to many microlumens.
(L) In FGF2-treated complex cysts, β1-integrin localizes to regions of cell-ECM contact, whereas ZO-1 localizes to luminal surfaces. Scale bars are 20 μm.

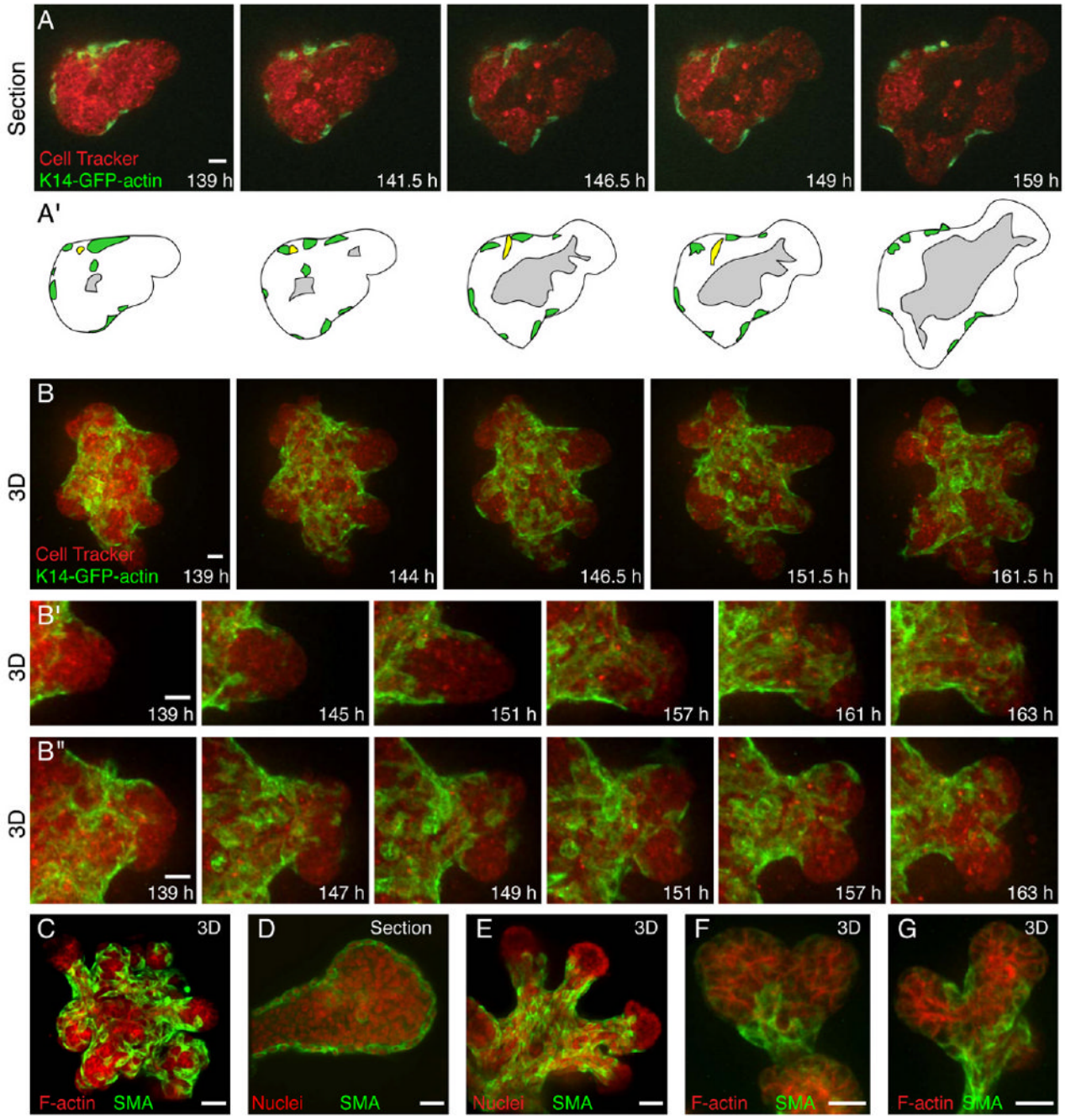

Figure 2. Myoepithelial Cells Move Actively during Ductal Elongation and Bifurcation

(A) Single-section frames from a time-lapse movie of ductal initiation and elongation in a K14-GFP-actin/CellTracker Red-labeled organoid (Movie S4).

(A′) Schematic view of (A); ME is green, and the lumen is gray. An ME cell (yellow) moves from a basal to an interior position.

(B–B″) 3D reconstructions of optical sections from a time-lapse movie of (B) ductal elongation and bifurcation (Movie S5) and, at higher magnification, (B′) ductal elongation and (B″) ductal bifurcation in a K14-GFP-actin/CellTracker Red-labeled organoid.

(C and E–G) 3D reconstructions of optical sections and (D) single optical sections of SMA-labeled ME in an (C) organoid, an (D) elongating duct, a (E) growth-arrested organoid, and (F and G) bifurcating ducts at higher magnification.
All images are from FGF2-treated organoids. Scale bars are 20 μm.

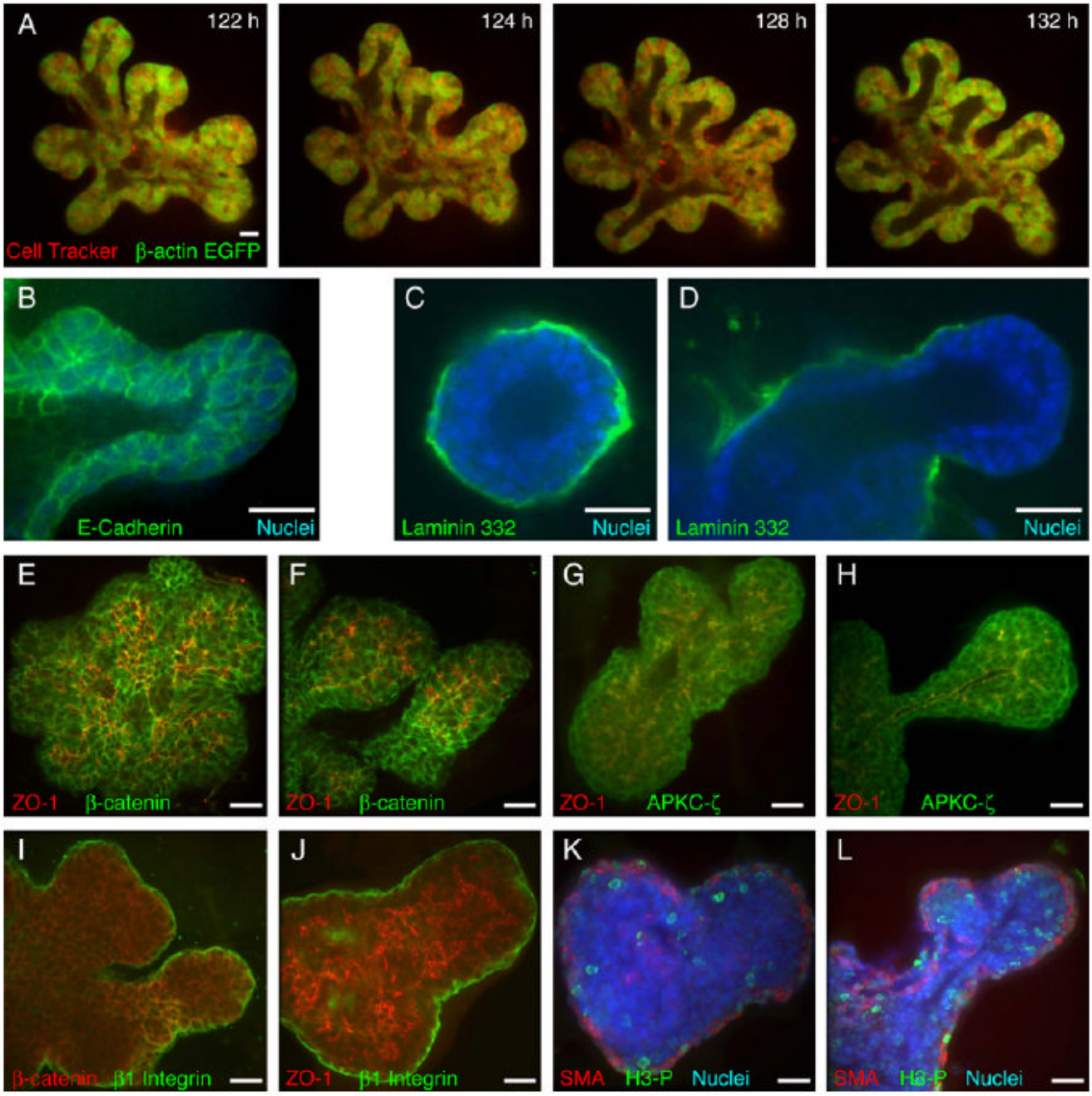

Figure 3. Mammary Epithelium Is Multilayered and Incompletely Polarized during Morphogenesis

(A) Single-section frames from a time-lapse movie of ducts stopping and repolarizing in a β-actin-EGFP/CellTracker Red-labeled organoid (Movie S6).

(B–H) Localization of (B) E-cadherin at cell-cell borders; laminin 332 in (C) unbranched organoids and (D) elongating ducts; β-catenin at lateral cell-cell boundaries, which is distinct from zona occludens 1 (ZO-1)-labeled apical surfaces during ductal (E) initiation and (F) elongation; and APKC-ζ at all apical and lateral cell-cell boundaries and colocalized with ZO-1 on apical surfaces during ductal (G) initiation and (H) elongation.

(I) β1-integrin at the basal cell-ECM border and localized to some β-catenin-labeled lateral cell surfaces.
(J) β1-integrin marks the basal tissue surface, and ZO-1 marks the apical tissue surface.
(K and L) Mitotic cells (phospho-histone H3+, H3-P) are widely distributed in both luminal and myoepithelial cell layers during (K) complex cyst and (L) ductal elongation phases.
All images are from FGF2-treated organoids. Scale bars are 20 μm.

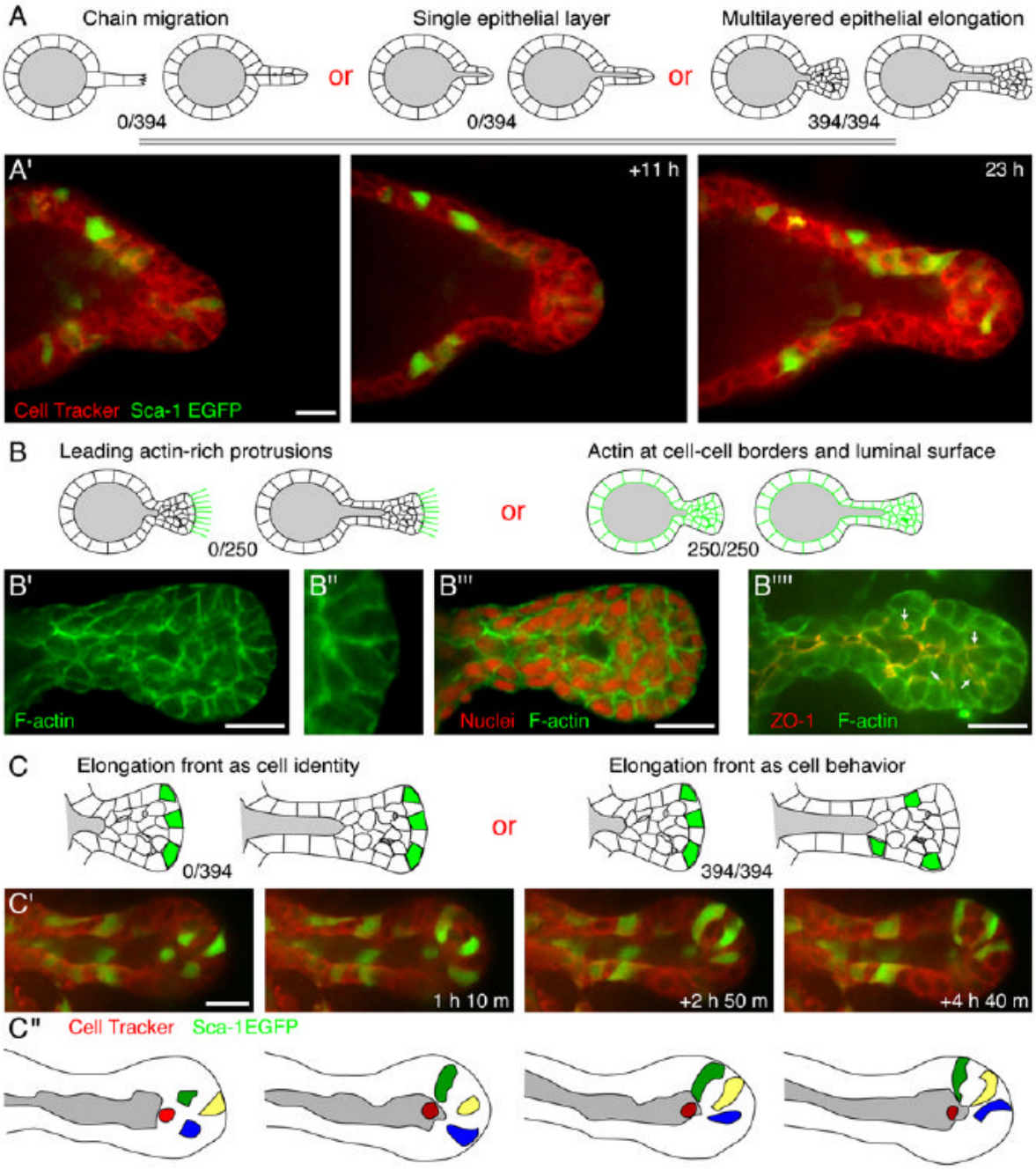

Figure 4. Ductal Elongation Occurs without Forward-Oriented Actin Protrusions in a Rearranging, Multilayered Cell Population

(A) Schematic of possible cellular mechanisms of ductal elongation.

(A′) Frames from a time-lapse movie showing multilayered epithelial elongation in a Sca-1-EGFP/CellTracker Red-labeled organoid (Movies S7 and S8).

(B) Possible localizations of F-actin in elongating ducts.

(B′–B‴) F-actin and nuclear localization in a representative elongating duct.

(B⁗) F-actin colocalizes with zona occludens 1 (ZO-1) along luminal surfaces.

(C) The cells at the elongation front could be constant (cell identity) or changing (cell behavior).

(C′) Frames from a time-lapse movie showing cell rearrangement during ductal elongation in a Sca-1-EGFP/CellTracker Red-labeled organoid.
(C″) Schematic view of the movie in (C′); individual cells are highlighted. The red cell shifts out of plane to the back surface of the lumen.
All images are from FGF2-treated organoids. Scale bars are 20 μm.

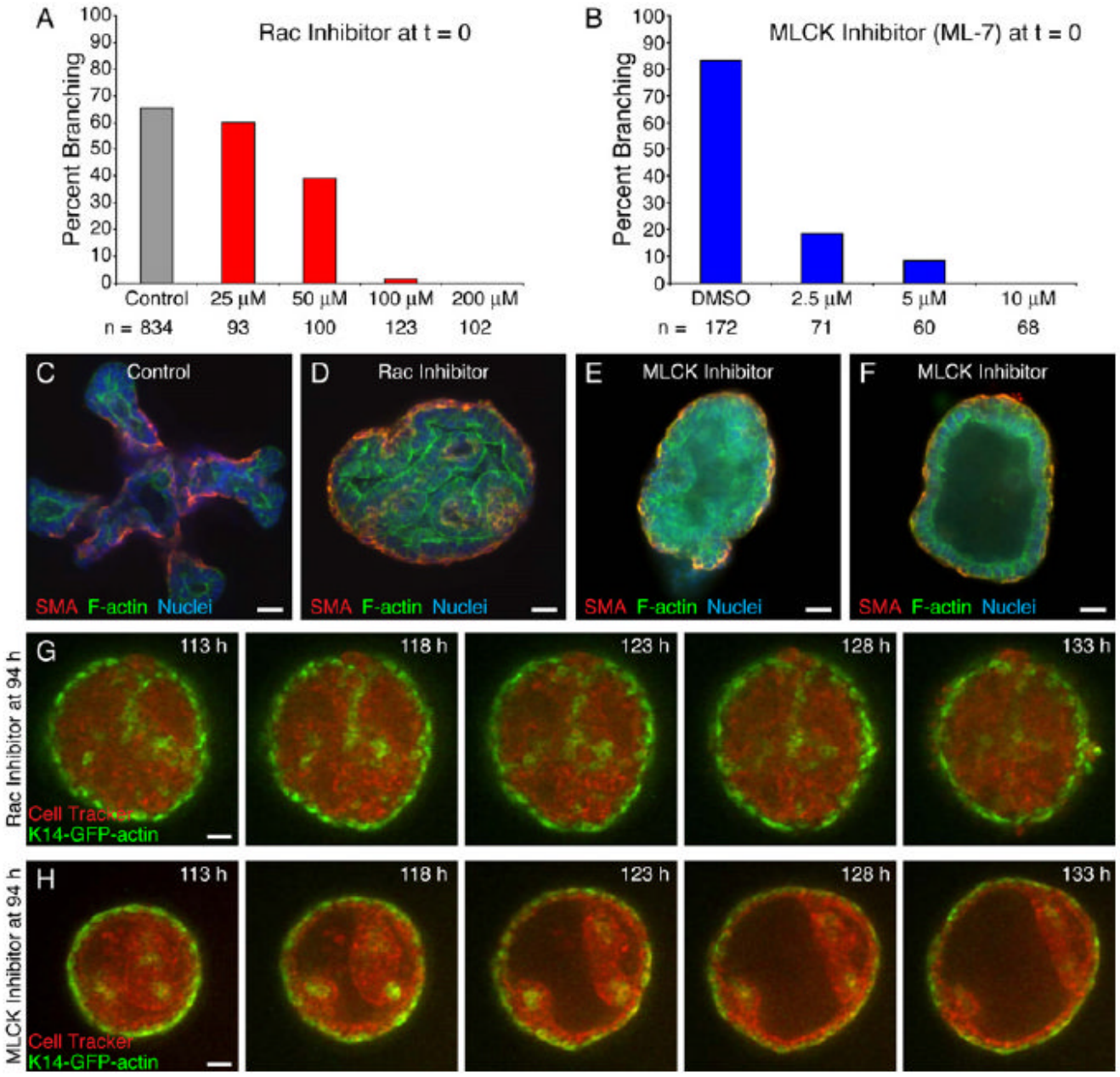

Figure 5. Rac-1 and MLCK Are Required for Ductal Initiation

(A and B) Inhibition of (A) Rac-1 and (B) MLCK causes dose-dependent inhibition of branching morphogenesis.

(C) The control organoid has initiated and elongated multiple new ducts.

(D) Rac-1 inhibition (100 μM, 0 hr) results in dense cysts with basal smooth muscle actin-positive (SMA+) myoepithelial (ME) cells and internal tubules.

(E and F) MLCK inhibition (4 μM, 0 hr) results in both (E) partially filled and (F) hollow cysts with basal ME.

(G and H) Frames from parallel time-lapse movies of a (G) Rac-1- (100 μM) (Movie S9) and (H) MLCK (5 μM) (Movie S10)-inhibited K14-GFP-actin/CellTracker Red-labeled organoid. All images are from FGF2-treated organoids. Scale bars are 20 μm.

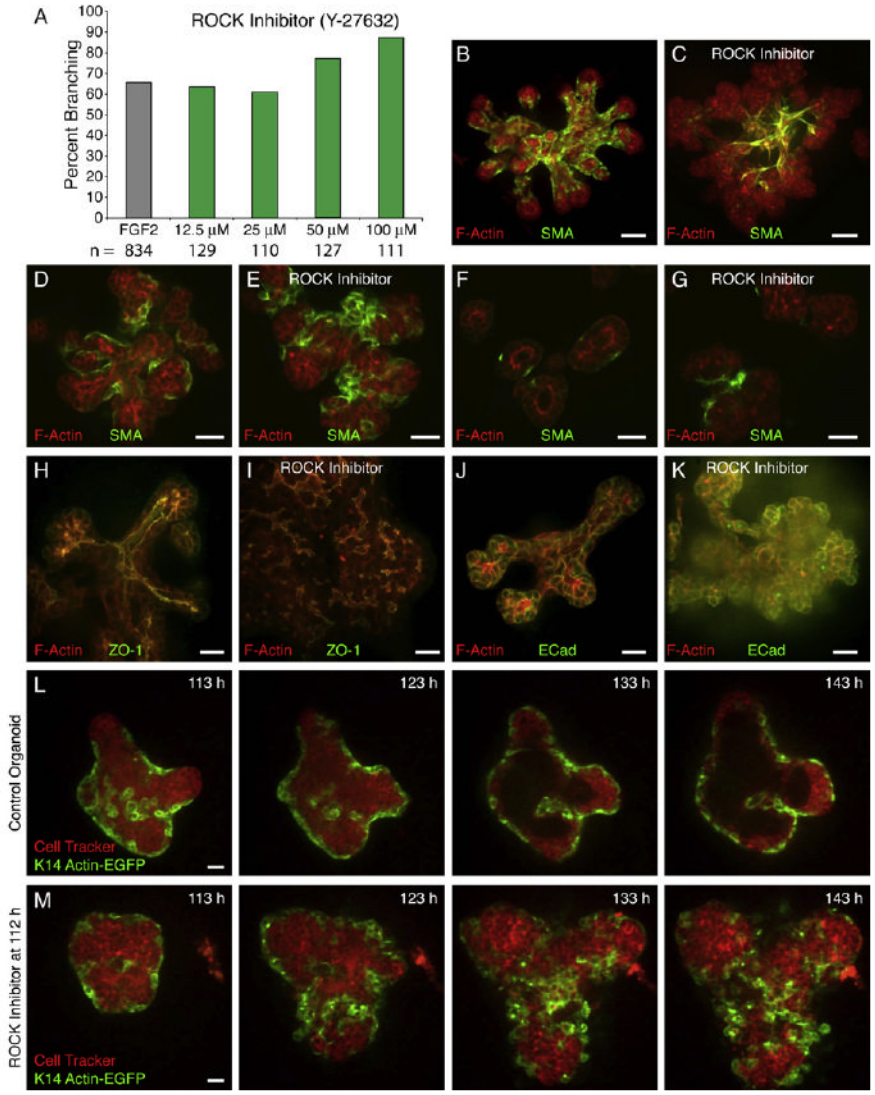

Figure 6. ROCK Signaling Is Required to Restore Simple Ductal Architecture

(A) Inhibition of ROCK does not prevent branching morphogenesis.

(B) Myoepithelial (ME) cells in control organoids are closely adherent and reflect the pattern of branching morphogenesis.

(C) ME cells in ROCK-inhibited organoids (50 μM) are disorganized, appear loosely adherent, and do not reflect the hyperbranched structure of the LE ducts.

(D and E) Longitudinal sections through (D) control and (E) ROCK-inhibited (50 μM) ducts.

(F and G) Transverse sections through (F) control and (G) ROCK-inhibited (50 μM) ducts.

(H and I) (H) Control organoids form large, connected, ZO-1-lined lumens, whereas (I) ROCK-inhibited organoids (50 μM) have fragmentary ZO-1-lined microlumens.

(J and K) Both (J) control and (K) ROCK-inhibited (50 μM) organoids localize E-cadherin to luminal cell surfaces.

(L and M) Frames from time-lapse movies, collected in parallel, of (L) control (Movie S11) and (M) ROCK-inhibited (Movie S12) (50 μM) K14-GFP-actin/CellTracker Red-labeled organoids.

All images are from FGF2-treated organoids. Scale bars are 20 μm.

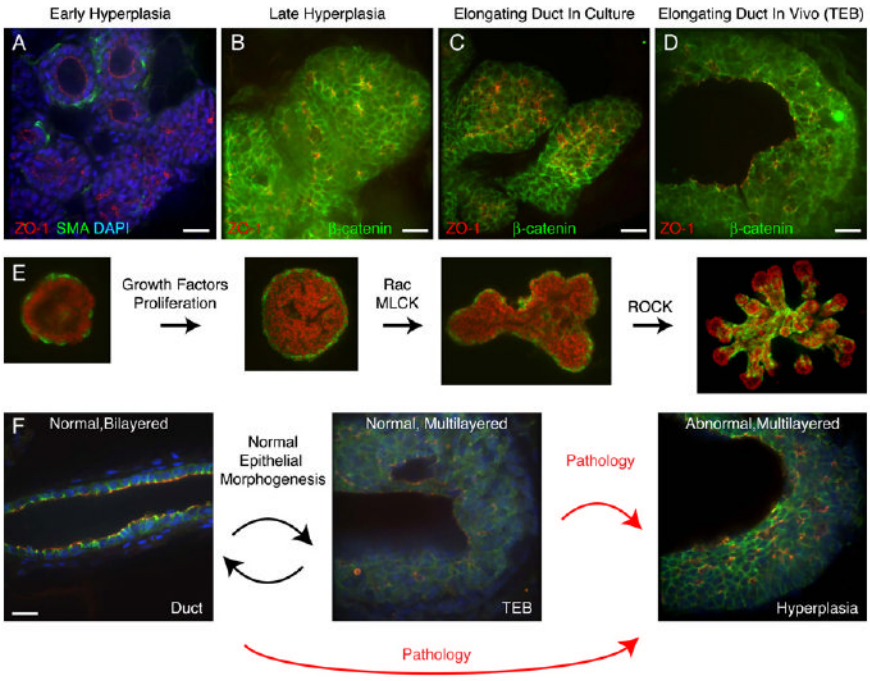

Figure 7. Mammary Epithelia Are in a Multilayered State during Morphogenesis

(A) Early hyperplasias from the MMTV-PymT mouse model lose myoepithelial (ME) coverage and transition into a multilayered epithelial organization.

(B) Late hyperplasias from the MMTV-PymT mouse model have a multilayered epithelial organization and consist of incompletely polarized cells, with β-catenin on all lateral surfaces.

(C and D) Normal (C) FGF2-treated ducts in culture and (D) terminal end buds in vivo are multilayered and consist of incompletely polarized cells, with β-catenin on all lateral surfaces.

(E) Schematic representation of epithelial morphogenesis in culture.

(F) During normal morphogenesis, mammary epithelium transiently reorganizes into a highly proliferative, low-polarity, multilayered state and then returns to a quiescent, simple epithelial state. Aberrant entry into, or failure to exit from, this morphogenetically active state may facilitate tumor initiation or progression.

Scale bars are 20 μm.